Plasma Chemistry and Plasma Processing
https://doi.org/10.1007/s11090-024-10497-1

ORIGINAL PAPER

Plasma Catalytic Non-Oxidative Conversion of Methane into Hydrogen and Light Hydrocarbons

Yonggang Gang[1] · Yanhui Long[1] · Kaiyi Wang[1] · Yilin Zhang[1] · Xuping Ren[1] · Hao Zhang[1,2] · Xiaodong Li[1]

Received: 29 November 2023 / Accepted: 1 August 2024

Abstract
Recently, direct non-oxidative conversion of methane (NOCM) into hydrogen and light hydrocarbons has garnered considerable attention. In our work, we employed a dielectric barrier discharge (DBD) plasma over a GaN/SBA15 catalyst for NOCM. Adding catalyst to plasma remarkably promotes the conversion of CH_4, resulting in a significant improvement, for instance, from 27.8 to 39.2%. A systematic investigation of plasma performance at different discharge powers with and without catalyst was conducted. In the case of plasma+15wt% GaN/SBA15, CH_4 conversion reaches an impressive 79.4%. However, it exhibits the lowest selectivity of 14.4% for C_2+, while achieving the highest selectivity for hydrogen at 48.9%. Several characterization methods, including XRD, SEM, BET, XPS, and TPO-MS, were used to study the mechanism of the reaction. Plasma electrons and ions can effectively interact with activated CH3 radicals, promoting their adsorption onto Ga sites on the catalyst surface. Simultaneously, hydrogen atoms adsorb onto neighboring N atoms, rapidly delocalizing to produce H_2, and the delocalization of hydrogen atoms in C species leads to the formation of species like CxHy. This study highlights the potential of plasma catalysis in significantly improving CH_4 conversion at lower temperatures and atmospheric pressure.

Keywords Non-oxidative methane conversion · Dielectric barrier discharge · Gallium nitride catalyst · Hydrogen · Light hydrocarbons

✉ Hao Zhang
zhang_hao@zju.edu.cn

✉ Xiaodong Li
lixd@zju.edu.cn

[1] State Key Laboratory of Clean Energy Utilization, Zhejiang University, Hangzhou 310027, China

[2] Ningbo Innovation Center, Zhejiang University, Ningbo 315100, China

Published online: 17 August 2024

Introduction

Climate change and energy depletion are the most serious challenges facing us today [1]. Due to the price fluctuations, and significant greenhouse gas emissions, natural gas is being increasingly recognized as a sustainable fossil fuel alternative and a valuable resource. There have been discovered to be substantial reserves of shale gas and methane hydrate [2]. Along with vast amounts of natural gas and waste/flamed methane, methane (CH_4) is a prolific source of hydrocarbons globally [3]. CH_4 is utilized to produce hydrogen and high-value light hydrocarbons, which helps to lower CO_2 emissions and improve the business by using cleaner resources throughout manufacturing. This viewpoint suggests that using methane is definitely one of the strategies that has to be implemented in order to achieve net zero emissions by 2050 [4].

Much research has been conducted on the conversion of CH_4 into useful chemicals, including syngas, methanol, light olefins, and aromatic compounds [5]. Syngas is a major feedstock for the chemical industry, since it is utilized to make a wide range of chemicals [6]. Converting methane directly to hydrocarbons may be more efficient and eco-friendly than producing syngas. Methane can be directly converted by oxidative coupling (OCM) [7, 8], non-oxidative dehydrogenation and aromatization (MDA) [9, 10], and non-oxidative conversion to oils, aromatics, and hydrogen (MTOAH) [11, 12]. The MTOAH route shows promise for CH_4 conversion to value-added light hydrocarbons and hydrogen with zero carbon dioxide emissions [13] However, the MTOAH process encounters two challenges. Firstly, the activity of the process is considerably low due to thermodynamic constraints. Secondly, the C-H bond (434 kJ mol^{-1}) is highly stable and poses difficulties in activation without the involvement of oxidation and catalytic processes [14].

Today, the majority of NOCM catalysts are based on Mo-zeolite systems, which mostly yield benzene and very little olefin [15–17]. With benzene as the main product (50–75%), zeolites containing molybdenum demonstrated the greatest CH_4 conversion (3–16%) [18]. Recently, Dumesic et al. [19]. developed PtSn-zeolite catalysts that achieve high C_2H_4 selectivity of 70–90% at 700 °C. Xiao and Varm [20] achieved a high ethane selectivity of 90% using bimetallic PtBi-zeolite catalysts, with a methane conversion of 1–5% at 700 °C. In the work of Bajec et al. [21]. , CH_4 conversion, C_2H_4 selectivity, and then coke of 1–6%, 50%, and 11–35 wt%, respectively were achieved by using Fe-Zeolite catalysts. At high temperatures (about 1000 °C), the active metal species, however, have a tendency to cluster into bigger nanoparticles and deactivate. Also, the methane conversion is only very limited (e.g., < 10%). Recent studies have shown that GaN can efficiently convert methane into light hydrocarbons with low coke yield. For example, Kopyscinski et al. [22–25]. found that GaN and GaN/SBA-15 convert methane to ethylene at above 650 °C, achieving around 5% methane conversion and 71% ethylene selectivity with low coke yield. Zhang et al. [26]. demonstrated GaN's high activity in the oxidative dehydrogenation of propane in CO_2. Thus, GaN is effective in C-H activation of light alkanes.

Non-thermal plasma (NTP) technology offers a viable substitute for the traditional catalytic process in converting CH_4 into chemicals and fuels with additional value [27]. Since plasma needs electricity to function, it may be powered by renewable energy sources like solar and wind. This would allow for safe, simple, lightweight, and flexible on/off switching. To effectively start chemical reactions, high-energy electrons and chemically reactive substances (like free radicals, ions) can be produced in NTP. NTP can have 1–10 eV electronic

energy and gas temperatures that are close to room temperature due to their strong non-equilibrium properties [28]. Because of this, NTPs are able to readily break most chemical bonds, including C-H bonds, and create environmentally favorable conditions for the occurrence of thermodynamically unfavorable chemical processes. Furthermore, the merging of plasma and catalysis has generated significant interest in ammonia synthesis, carbon nanomaterial development, environmental purification, greenhouse gas reformation, and catalyst treatment [28–34]. The combined action of plasma and catalysts can activate the catalyst at lower temperatures, increase its stability and activity, and eventually improve the target product's conversion, selectivity, and yield. Additionally, this integration may increase the plasma process's energy efficiency [28]. To date, the NOCM through various NTPs (with or without catalysts) has been the subject of extensive research, including dielectric barrier discharges (DBD) [35, 36], pulse discharges [37, 38], spark discharges [39], radio-frequency discharges [40], corona discharges [41], microwave discharges [42], and nanosecond pulse discharges (NPD). [43] After conducting a techno-economic analysis that considers various factors, including the electricity supply, it was found that using plasma pyrolysis of methane to produce hydrogen with renewable energy sources results in much lower CO_2 emissions compared to other methods [44]. However, the efficient conversion of CH_4 and high selectivity towards hydrogen and high-value-added light hydrocarbons still pose significant challenges, thereby necessitating the integration of both catalyst and plasma to explore a promising pathway.

DBD is created by applying an electric potential between two electrodes, where at least one is covered by a dielectric barrier. Methane conversions of between 1% [45] and 47% [46] were reported at room temperature, with a specific energy input (SEI) ranging from 0.1 to 300 kJ L^{-1}. Ethane (C_2H_6) typically is formed as the main product, followed by other C2 hydrocarbons, C3-C5 compounds, and soot with varying selectivity [47]. Scapinello et al. [48]. found that Xu and Tu [35] achieved the best results about CH_4 conversion in a DBD. They found that the CH_4 conversion rate was 11%, the C_2H_6 selectivity was 34%, the selectivity for other C2 hydrocarbons was 19%, and the remaining components were soot and C3–C4 hydrocarbons. However, Lower conversion and selectivity, as well as uncertain processes of plasma-catalyst interactions, remain problems for the DBD. More specifically, to optimize light hydrocarbon formation, we need to understand more about the key chemical pathways.

In this work, we investigated GaN-SBA15 with varying Ga loading for converting CH_4 into light hydrocarbons and H_2 using DBD under normal pressure and low temperature conditions. We observed significant improvement in CH_4 conversion with plasma catalysis compared to plasma only. The introduction of plasma lowers the catalyst's active temperature by electrically impacting its surface. The study proposed a possible reaction mechanism for CH_4 conversion with plasma and a catalyst, which helps to understand the synergy between plasma and catalysts. The mechanism was determined through catalyst characterization and product analysis.

Experimental

Experimental Setup

The experimental setup for the plasma-catalytic methane conversion is shown in Fig. 1. A coaxial DBD reactor with a discharge zone length of 40 mm and a discharge gap of 2.5 mm was used for the experiment. The reactor operates at atmospheric pressure. A 20 kV peak voltage and 10 kHz frequency high-voltage AC power supply are connected to the DBD reactor. A soap film flow meter was used to calibrate the reactant gas, which was CH_4 in Ar at a molar ratio of 1:19. The overall flow rate was 100 mL/min. A catalysis weighing 0.5 g is placed inside the discharge region. During the plasma-catalytic methane conversion experiment using GaN/SBA15 as a catalyst, gas products were sampled every 20 min over 1 h to evaluate the performance of catalysts under various working conditions. The voltage and current of the DBD were measured using a high-voltage probe (TESTEC, HVP-15HF) and a current monitoring loop (Bergoz, CT-E0.5), respectively. The electrical signals were captured and recorded using a four-channel digital oscilloscope (RTM3000,R&S). The Q-U Lissajous method was used to compute the discharge power. The reaction products were examined using a gas chromatographic system (GC9790 PLUS, FULI INSTRUMENTS) fitted with FID and TCD detectors. After three iterations of the experiment, the uncertainty was found to be within 4%.

Catalyst Preparation and Characterization

The detailed process of catalysis synthesis was carried out as follows, hydrochloric acid (36–38% HCl, Fisher Chemical) and deionized water were used to dissolve P-123 copolymer. To make sure the copolymer was well dissolved, the mixture was agitated for several hours at normal atmospheric temperature. After that, tetraethoxysilane (TEOS, 98%, ACROS) was added and stirred for a full day at 600 rpm. In closed polypropylene Digi-

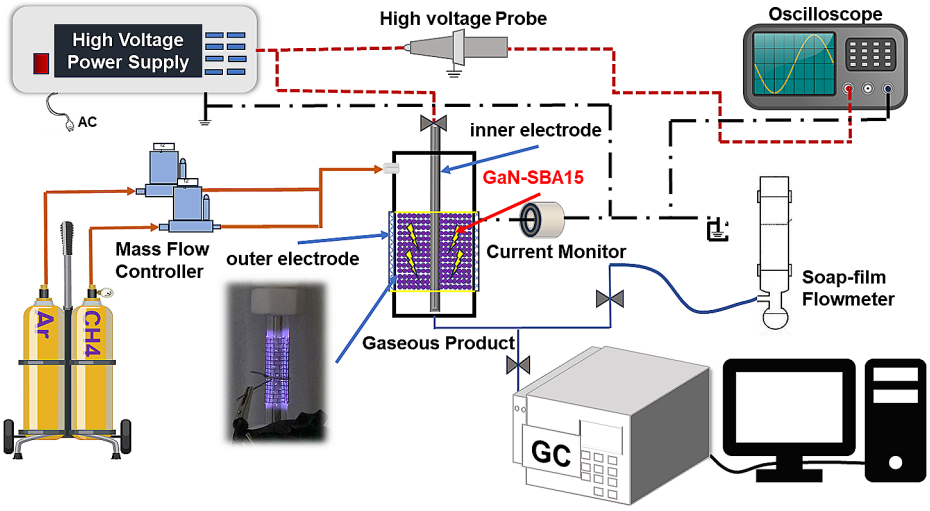

Fig. 1 Schematic of the plasma-catalysis experimental system

TUBEs (SCP SCIENCE), the opaque white solution was hydrothermally treated for 48 h at 100 °C. The precipitate was then recovered after filtering. Deionized water was used to wash the precipitate multiple times. To produce SBA15, the precipitate was dried overnight at 60 °C, transferred to a ceramic boat and then calcined at 550 °C for 6 h (1 °C min^{-1}) The initial impregnation approach was used to prepare the supported catalyst. The precursor of Ga was dry gallium (III) nitrate hydrate powder (Ga $(NO_3)_3$ $6{\cdot}H_2O$, Aladdin). The amount of precursor required to reach the 16 wt% goal load Stoichiometry was utilized to calculate Ga. The first impregnation in deionized water is done using the aqueous nitric acid solution. 1 g of SBA15 required roughly 4.5 ml of the solution. The wet solid was impregnated, allowed to stand at normal atmospheric temperature for the entire night, and dried for eight hours at 60 °C. Lastly, the dry solid was labeled with Ga_2O_3/SBA15 and calcined for 6 h at 550 °C (1 °C min^{-1}). Ga_2O_3/SBA15 was nitrided for 6.5 h with ammonia (NH_3, 99.99%, Meg's special gas, 50 mL min^{-1}) in a fixed-bed reactor at 750 ℃, and then cooled to room temperature under continuous NH_3 flow. The prepared GaN/SBA15 sample was yellow powder, and the experiment was carried out after granulation.

Nitrogen adsorption/desorption measurements were used to physically characterize the produced catalysts. Total surface area, pore size distribution, and pore volume were among the parameters examined. The Brunauer-Emmett-Teller (BET) method was used to calculate the surface area, and the Barrett, Joyner, and Halenda (BJH) method was used to study the mesoporosity. A fully automated BET (Quantachrome Autosorb IQ3, USA) specialized surface and porosity analyzer was used for the measurements. The samples were degassed under vacuum for 12 h at 250 °C before analysis. Using Cu target radiation (X-ray generator power 3 KW, new 9 KW rotating target), powder X-ray diffraction (XRD) investigations were performed on a Rigaku SmartLab SE diffractometer. A rate of 1 °/min was used to record X-ray diffractograms between $2\theta = 5–90°$. A German-made ZEISS Sigma 300 field emission scanning electron microscope was used to analyze fresh and spent loaded gallium nitride samples using scanning electron microscopy (SEM). Additionally, mapping tests were carried out to examine the distribution of the elements (carbon, nitrogen, oxygen, and gallium) in the samples. Al Ka radiation was used for X-ray photoelectron spectroscopy (XPS) (Thermo Scientific K-Alpha, USA). A 284.8 eV C1s signal was used to calibrate the binding energies for all of the spectra. For each spent catalysis, high-resolution area scans and low-resolution surveys were carried out to determine the binding energies involved. Using inductively coupled plasma optical emission spectroscopy (ICP-OES, Agilent 5110, USA), the gallium concentration of the loaded catalysis GaN/SBA15 was ascertained. For both fresh and spent catalysis, temperature-programmed oxidation mass spectrometry (TPO-MS) analysis was used to measure the quantity of coke deposited (and carbon inherent in the fresh catalyst, if any). A reaction tube containing 30–40 mg of sample was filled, weighed, and set to warm at a rate of 10 °C/min from room temperature to 110 °C for drying pretreatment. The tube was then cooled to 50 °C, purged by He air flow (50 mL/min) for one hour, and passed through a 10% O_2/He mixture (50 mL/min) for one hour until saturation. Finally, the tube was warmed under a 10% O_2/He mixture at a ramp-up rate of 10 °C/min. Ultimately, the gas was discovered by TCD when it was desorbed at 950 °C under a 10% O2/He mixture at a temperature increase rate of 10 °C/min.

Calculation Method

The conversion of CH_4 (X_{CH4}) is defined as

$$X_{CH_4}(\%) = \frac{moles\ of\ CH_4\ converted}{moles\ of\ initial\ of\ CH_4} \times 100 \quad (1)$$

The selectivity of gaseous products (H_2 and C_mH_n) is calculated according to Eqs. 2–3

$$S_{H_2}\ (\%) = \frac{moles\ of\ H_2\ produced}{2 * moles\ of\ CH_4\ converted} \times 100\% \quad (2)$$

$$S_{C_mH_n}\ (\%) = \frac{m * moles\ of\ C_mH_n\ produced}{moles\ of\ CH_4\ converted} \times 100\% \quad (3)$$

The energy efficiency is defined as Eq. 4, which is expressed as moles of gas per unit of plasma power converted

$$energy\ efficiency\ \left(mmol \cdot kWh^{-1}\right) = \frac{converted\ product\ \left(mmol \cdot h^{-1}\right)}{discharge\ power\ (kW)} \quad (4)$$

The specific energy input is defined as

$$SEI\ \left(kJ\ L^{-1}\right) = \frac{P_{tatal}}{Q_{gas}} \quad (5)$$

Where $P_{(tatal)}$ is the discharge power of the reactor as measured by an oscilloscope and $Q_{(gas)}$ is the gas flow rate into the reactor.

$$C_{balance} = \frac{[moles\ of\ CH_4]_{out} + \sum m * moles\ of\ C_mH_n\ produced}{[moles\ of\ CH_4]_{in}} \times 100\% \quad (6)$$

Where [moles of CH_4] $_{in}$ and [moles of CH_4] $_{out}$ represent the moles of methane before and after reactions, respectively.

Result and Discussions

Reaction Performance

The CH_4 conversion and product selectivity of the plasma-only, plasma+SBA15, and plasma+GaN/SBA15 cases under different discharge powers are presented in Fig. 2. The discharge power affects strongly the CH_4 conversion. For instance, increasing power from 28 W (SEI=17.2 kJ/L) to 42 W (SEI=25.7 kJ/L) improves the CH_4 conversion from 27.8 to 39.7% in the plasma-only case. Notably, the introduction of catalyst and plasma also enhances the CH_4 conversion, especially at higher discharge powers. The introduction of SBA15 does not noticeably affect the CH_4 conversion (from 21.5 to 20.5%) at a power of 20 W while employing GaN/SBA15 enhances slightly the CH_4 conversion (from 21.5 to 23.8%). However, the CH_4 conversion at plasma+GaN/SBA15 case enhances remark-

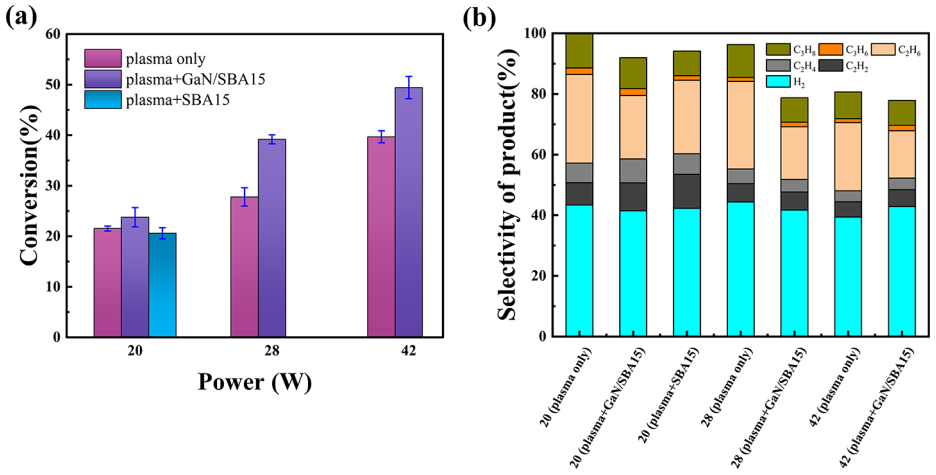

Fig. 2 (**a**) CH_4 conversion and (**b**) product selectivity for the Plasma only, Plasma+SBA15, and Plasma+GaN/SBA15 with different discharge power, (20 W, 28 W, 42 W respectively), Reaction conditions: WHSV 12,000 $mlg^{-1}h^{-1}$, CH_4/Ar molar ratio of 1:19, discharge frequency of 10 kHz, and 1 h reaction time

ably from 27.8 to 39.2% at a power of 28 W and from 39.7 to 49.4% at a power of 42 W respectively. Moreover, plasma-catalysis, for instance, improves energy efficiency from 4.3 to 5.2% at 28 W. Catalysis and discharge power are responsible for the improvement in CH_4 conversion. The gas-phase reaction may have contributed to the discharge power, and the addition of the GaN/SBA15 catalyst played a significant part in the NOCM, underscoring the catalysis's importance in optimizing the conversion process.

The amount of filler present in the discharge affects the strength of the electric field. GaN/SBA15, a material with a higher dielectric constant, has a greater impact on the electric field of the electric discharge [49]. A typical filamentary discharge occurs without any filler present. However, the gas void is considerably reduced when GaN/SBA15 is used to cover the entire discharge gap. The discharge zone experiences a decrease in filamentary discharge and an increase in surface discharge on the catalysis. Studies conducted on packed-bed DBD reactors, both through experiments and modeling, have demonstrated this [50, 51]. The difference in reactivity between plasma+GaN/SBA15 and plasma+SBA15 implies that the function of GaN/SBA15 may involve both gas-phase reactions and plasma-assisted surface reactions that facilitate the conversion of CH_4 [52, 53]. When the discharge power was raised, the CH_4 conversion of plasma-only was comparable to that of GaN/SBA15, suggesting that the weak discharge was ineffective for methane conversion. The peak-to-peak charge rises in tandem with the discharge power. With increasing discharge power, more charges are produced and transmitted each half-cycle of applied voltage [49]. The packing elements introduced to the DBD reactor have a major effect on the charge parameters of the CH_4 discharge. A prior investigation during plasma methane reforming shown an increase in charge parameters with discharge power [54].

The selectivity of each product for different conditions is shown in Fig. 2, which suggests that the catalyst was involved in homogeneous CH_4 activation, activating CH_4 to form CH_3 radicals and acting on subsequent reaction pathways [53]. This supported the experimen-

tal findings that carbon was deposited and high carbon hydrocarbons formed in the inner electrode and wall during the experiment, and it also showed the existence of high hydrocarbons (C4+) as a result of additional chain growth and cyclization. According to these results, increased methane conversion without catalysis does not result in more carbon formation. Moreover, at the same discharge power, plasma+GaN/SBA15 showed lower light hydrocarbon selectivity than plasma alone, while H_2 selectivity remained unchanged. This phenomenon was attributed to the result of the filler on the discharge characteristics and the contribution of the catalysis on the reactant reaction path.

For the plasma catalysis reaction, more research was done on the impact of GaN loading on reaction performance. As displayed in Fig. 3, the performance in plasma-catalysis cases remarkedly increased with a 15 wt% loading, surpassing that of the plasma and catalysis by a significant margin (79.4%). This demonstrates that varying the loadings of gallium metal can significantly influence CH_4 conversion. However, the plasma with 15 wt% GaN/SBA15 catalyst has a lower selectivity of 14.4% for C_2+, which is nearly half the reduction (up to 32.5%) and the highest selectivity for hydrogen (up to 48.9%). Except at 15 wt% where it was 77.6%, the Carbon balance for the catalyst was around 90% at different metal loadings. This suggests that there was more carbon deposition and high carbon hydrocarbon in the plasma+GaN/SBA15 case.

The DBD plasma GaN/SBA15 catalyst demonstrated high conversion efficiency and low-temperature (<200°C) catalytic activity. Additionally, the plasma activation temperature for CH_4 on GaN/SBA15 was lower than that of previously reported thermal catalysis [24]. Even though the selectivity of C_2+products is slightly lower compared to high temperatures, this work on the plasma GaN/SBA15 catalyst shows that it has a high CH_4 conversion rate at lower temperatures, which is competitive with the rates reported in the literature [55]. This presents a potential approach toward the non-oxidative coupling of CH_4.

Catalyst Characterization

The morphology and elemental mapping of fresh (GaN/SBA15-fresh) and used GaN/SBA15 catalysis (GaN/SBA15-spent) with plasma were analyzed to interpret the mechanisms. Both GaN/SBA15-fresh and GaN/SBA15-spent had a 15% gallium metal loading. The homoge-

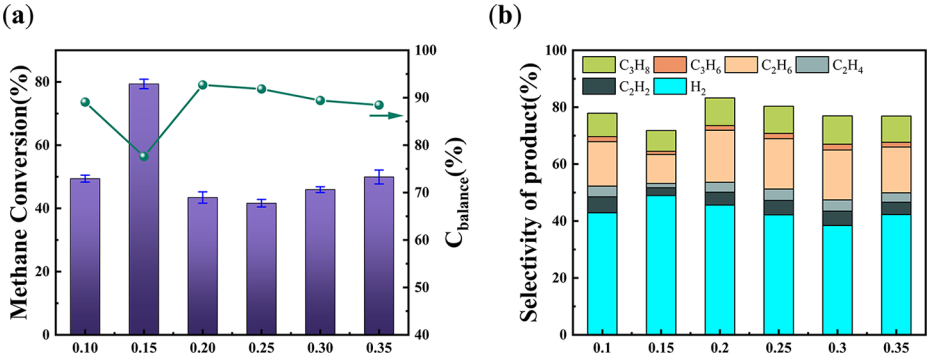

Fig. 3 **(a)** CH_4 conversion, C balance and **(b)** product selectivity plots of plasma+GaN/SBA15 with different gallium metal loadings (10 wt%, 15 wt%, 20 wt%, 25 wt%, 30 wt%, 35 wt% respectively), Reaction conditions: WHSV 12,000 $mlg^{-1}h^{-1}$, CH_4/Ar molar ratio of 1:19, discharge frequency of 10 kHz, and 1 h reaction time

neous distribution of both Ga and N species was confirmed by the magnified SEM images and accompanying elemental mapping, despite the nonuniform particle shape. According to previous studies, it has been well-established that a substantial proportion of the GaN nanoparticle surfaces are predominantly constituted by the c-planes (0001) and m-planes (1100) [56]. GaN's symmetrical structure, with equimolar Ga and N atoms organized in a tetrahedral coordination configuration, is responsible for the material's intrinsic nonpolar nature in the m-plane. Conversely, the polar c-plane, which can only accommodate one kind of atom (Ga or N), is what causes piezoelectric polarization along the c-axis. (Fig. 4). [22] Significantly, it is worth mentioning that a minor quantity of carbon species was discerned, primarily arising from surface-adsorbed carbon [57]. The distribution of N and C elements is visible under plasma-catalyzed circumstances (Fig. 4b–d), in addition to the distribution of gallium (Ga) elements. This strongly suggests that gallium metal is actively involved in the methane conversion process.

Table 1 presents the findings of measuring the specific surface areas (S_{BET}) of the produced samples using N_2 adsorption-desorption isotherms. The S_{BET} of 575 m^2g^{-1} was comparatively high for the SBA15 support. However, after the support was impregnated with gallium and underwent nitridation, over 50% of the overall surface area was lost, going

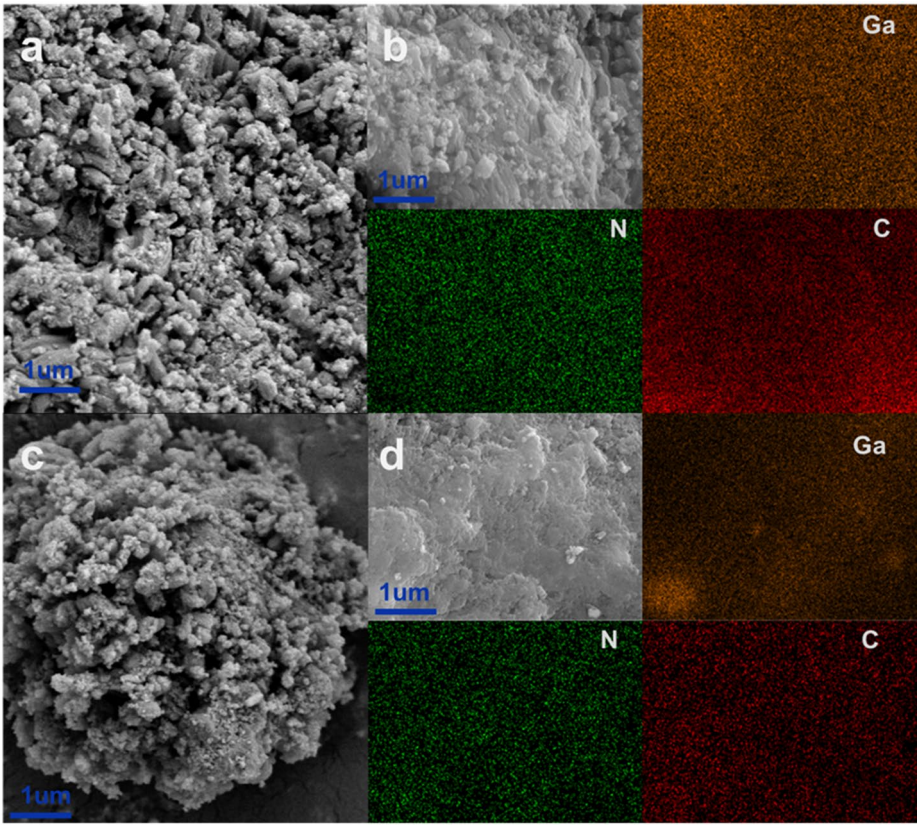

Fig. 4 (**a, c**) SEM images and (**c, d**) the corresponding EDS mappings for the GaN/SBA15 catalyst; (**a–b**) the fresh catalyst; (**c-d**) the spent catalyst

Table 1 Physicochemical properties of the catalysis

Sample	Carbon content (%)	Carbon amount (mmol/g)	Surface Area (m^2g^{-1})	Pore Diameter (nm)	Pore Volume (cm^3/g)
SBA15	--	--	575	7.9	0.89
GaN-SBA15-fresh	6.87	0.145	232	11.9	0.55
GaN-SBA15-spent	18.65	0.893	287	9.3	0.58

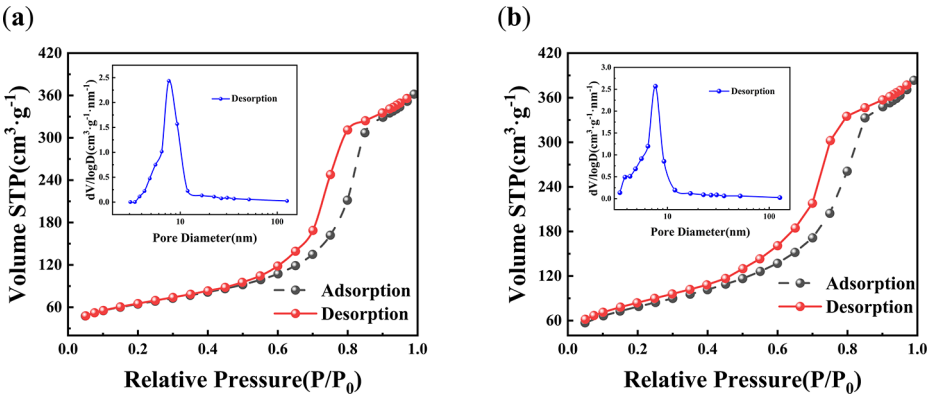

Fig. 5 N_2 sorption isotherms and pore diameter distribution of GaN/SBA15-fresh (**a**) and GaN/SBA15-spent (**b**)

from 575 m^2g^{-1} to 232 m^2g^{-1}. This significant decrease resulted from the pore structure collapsing and GaN crystallization beginning, which was triggered by the high temperatures encountered during the calcination procedure. The higher deposition of carbon and plasma treatment on the GaN/SBA15 Spent surface are the main reasons for the S_{BET} value (287 m^2g^{-1}), which is clearly observed after the CH_4 transformation and is significantly higher than the GaN/SBA15-fresh value [58]. Figure 5 shows the catalysis's nitrogen adsorption-desorption isotherms and pore diameter distribution. Typical type III isotherms are observed in GaN/SBA15, suggesting the presence of a large mesoporous or macroporous structure [59]. The porosities virtually inside the mesoporous domains are also shown by the matching pore size distribution. (Fig. 5). It is evident that both fresh and spent catalysis have almost identical specific surface areas both before and after plasma. On the other hand, a slight variation in the distribution of pore diameter was observed, most likely due to the positioning of GaN nanoparticles within their pores [60].

The GaN/SBA15 catalyst's gallium content was verified analytically using inductively coupled plasma optical emission spectroscopy (ICP-OES), a dependable method. The obtained analytical findings revealed an actual gallium content of 14.1%, which closely approximates the expected theoretical yield of 15.0 wt%. The small deviation from the expected value of about 1 wt% can be attributed to the inherent loss of mental that may occur during catalyst synthesis.

XRD patterns of the fresh and spent catalysts are illustrated in Fig. 6. The diffraction peaks of GaN were found at $2\theta = 32.5°$, 34.6°, 37.0°, 48.3°, 57.9°, 63.7°, and 69.1°. These

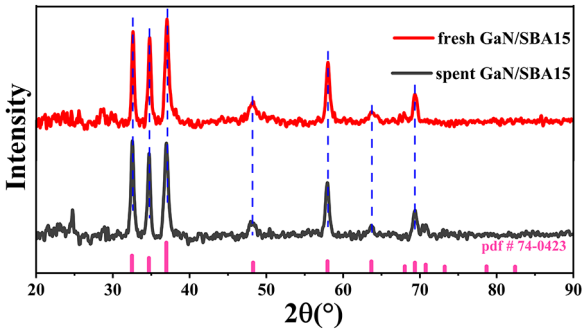

Fig. 6 XRD patterns of GaN/SBA15 catalysts

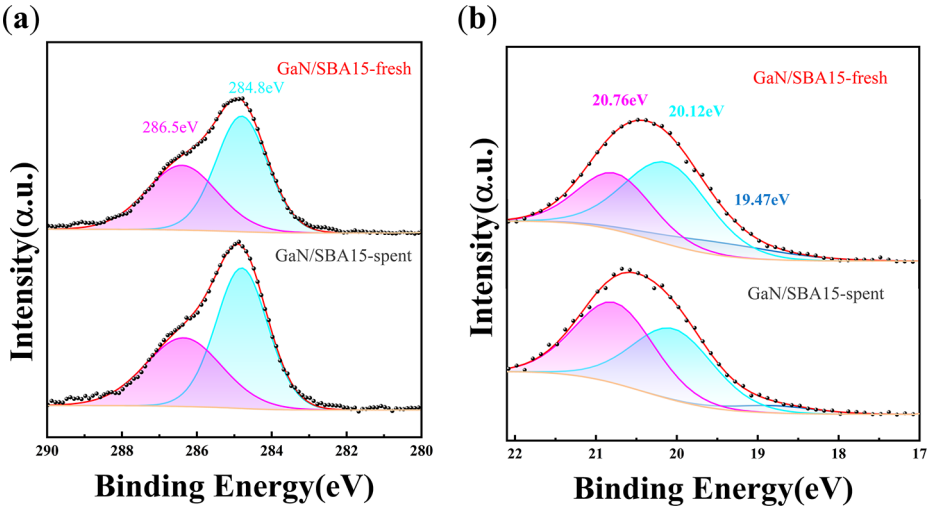

Fig. 7 The XPS spectra of C 1s (**a**) and Ga 3d (**b**) of GaN/SBA15 catalysts before and after methane conversion

match to the planes of the wurtzite structure GaN (PDF#74–0243) and the (100), (002), (101), (102), (110), (103), and (201) [60]. GaN/SBA15-spent's diffraction pattern showed strong similarities to that of GaN/SBA15-fresh, albeit with weaker amplitudes. This suggests that there are smaller GaN crystallites and more amorphous phases present, which may be related to the contribution of plasma on the GaN particles during NOCM. While there were indications of crystalline GaN in the nitridated gallium-containing supported catalysts, there were no observable peaks corresponding to Ga_2O_3, suggesting that the latter was a noncrystalline particle. The amorphous Ga_2O_3 was transformed into crystalline GaN during the nitridation. This led to the appearance of distinct and well-defined peaks in the diffraction pattern, which matched the crystalline structure of GaN. [24]

The XPS spectra of C 1s and Ga 3d for the fresh and spent GaN/SBA15 samples are displayed in Fig. 7. The Ga 3d XPS photolines in the GaN/SBA15 (Fig. 7b) XPS spectra were positioned at around 20.0 eV and could be further divided into three peaks at 20.76 eV, 20.12 eV, and 19.47 eV. The Ga-O bond was found to be the peak at 20.76 eV, and the Ga-N bond was found to be the highest at 20.12 eV. The remaining peak was linked to the N 1s

core level and was situated at 19.47 eV [61]. The imperfect conversion of gallium oxide to GaN during nitriding is responsible for the presence of the Ga-O bond, which was maintained in part in the final catalyst. Furthermore, the XPS spectra of Ga 3d reveal an intriguing finding: the Ga-N bond peak intensity in GaN/SBA15-spent was marginally weaker than in GaN/SBA15-fresh. This finding offers strong proof that gallium does, in fact, essential to the NOCM. These observations match the findings from the SEM and XRD analyses. Table 2 shows the surface compositions of both fresh and spent. The concentrations of Ga and N of each catalyst were lower than their respective bulk composition, while the concentrations of C and O were observed to be higher than the bulk composition, indicating that the GaN/SBA15-spent surface was enriched with C and O [56].

C 1s XPS spectra (Fig. 7a) was examined to determine the kind and generation of the carbon deposits. The graphitized carbon's C-C bond is responsible for the peak at 284.8 eV in the fresh samples, whereas the C-O bond is linked to the peak at 286.5 eV. The adsorption of tainted carbon from the measurement apparatus or CO_2 and H_2O in the ambient air may create the C-O bond. Both GaN/SBA15-fresh and GaN/SBA15-spent exhibited identical carbon coordination structures. The peak strength associated with the C-C bond increases slightly in the GaN/SBA15 spent sample, confirming the deposition of carbonaceous material during CH_4 conversion. It is indicated that methane does not excessively build up carbon in plasma-only and plasma-catalytic conditions. The C-O bond remains, mainly due to the adsorption of carbonaceous material from the air.

The amount of carbon adsorbed during methane conversion was estimated using temperature-programmed oxidation mass spectrometry (TPO-MS) analysis of both new and spent catalysts. As summarized in Table 1 and displayed in Fig. 8, in agreement with the SEM-EDS data, the TPO-MS results indicated that the total amount of fresh GaN/SBA15 was 0.145 mmol/g. Concurrently, a higher carbon content (0.893 mmol/g) was found for the spent GaN/SBA15, but marginally lower than the 18.65% SEM-EDS values. This is because the catalyst has a large amount of carbon which is not evenly distributed but rather has a random distribution. The samples that were supported performed better because they had higher conversion for CH_4 and adsorbed less carbon. In addition, the result of TPO-MS showed the types of deposited carbon. TPO-MS showed a single 350 °C CO2 peak for both fresh and spent catalysts; amorphous carbon was responsible for the weight loss between 380 and 520 °C, whereas filamentary carbon was responsible for the weight loss between 520 and 720 °C [62, 63]. It was challenging to gasify or remove the burned graphitic carbon, which was the cause of the weight loss at temperatures above 720 °C. [62] Based on the results, it was found that the majority of the carbon that was adsorbed existed in an amorphous state as opposed to a graphite state. Nevertheless, the specific type and stoichiometry of the adsorbed carbon (CxHy) remains unknown. It is expected that the deposition of these carbon species will lead to a decline in the catalytic activity of GaN/SBA15.

Table 2 Elements present on the surface as determined by the XPS spectroscopy

Sample	Atomic percentage (%)				
	Ga	N	C	Si	O
GaN-SBA15-fresh	4.89	3.63	7.44	29.03	55
GaN-SBA15-spent	4.77	3.62	8.98	28.73	53.85

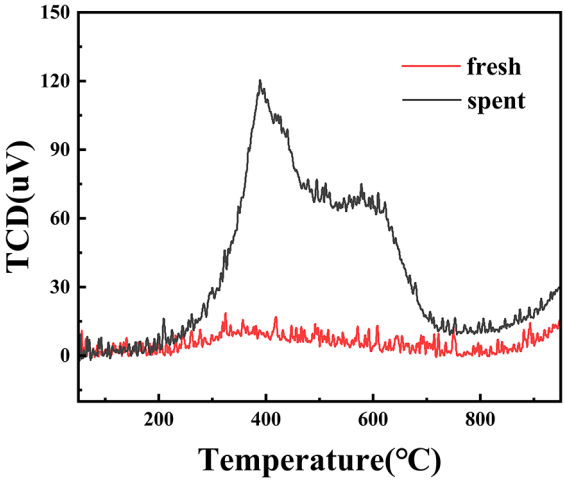

Fig. 8 TPO-MS for fresh GaN/SBA15 and spent GaN/SBA15 catalysts for methane non-oxidative conversion at DBD

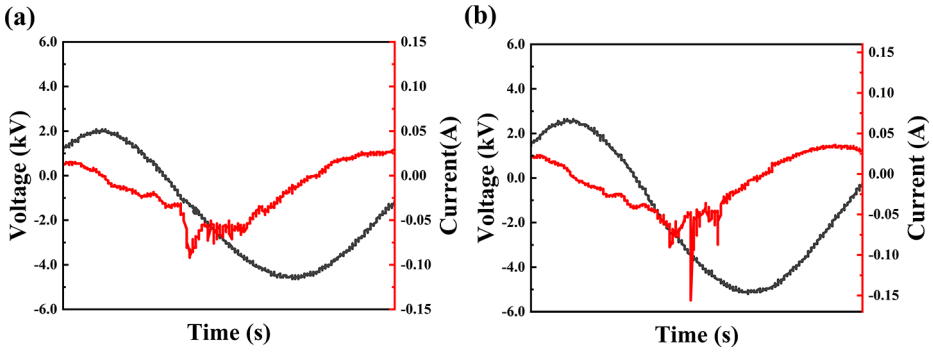

Fig. 9 U-I figures of plasma only (**a**), packed with GaN/SBA15 (**b**)

Reaction Mechanisms

Two factors—the strong coupling between the plasma and the catalyst and the catalyst's addition, which changed the discharge field strength—are responsible for the notable improvement in CH_4 conversion in the plasma+catalysis example. As seen in Fig. 9, to better understand the characteristics of the discharges created in the various reactor designs, electrical diagnostics were carried out and different discharge parameters were estimated using electrical signals in conjunction with the U-I values.

The following plan for the CH_4 activation to H_2 and light hydrocarbons is offered based on the experimental results and the current density functional theory (DFT) analysis, as shown in Fig. 10. [58, 64] Gallium-nitrogen and gallium-oxygen atom pairs facilitate the dissociation of methane into an alkyl (CH_3) and hydrogen (H) via the alkyl pathway [22]. The plentiful CH_3, CH_2, CH, and H radicals were produced by the cracking of CH_4 molecules upon the injection of plasma. The radicals generated by plasma and CH_4 undergo quick dissociative chemisorption on GaN. CH_3* adsorbs onto Ga^{3+} while H* adsorbs onto

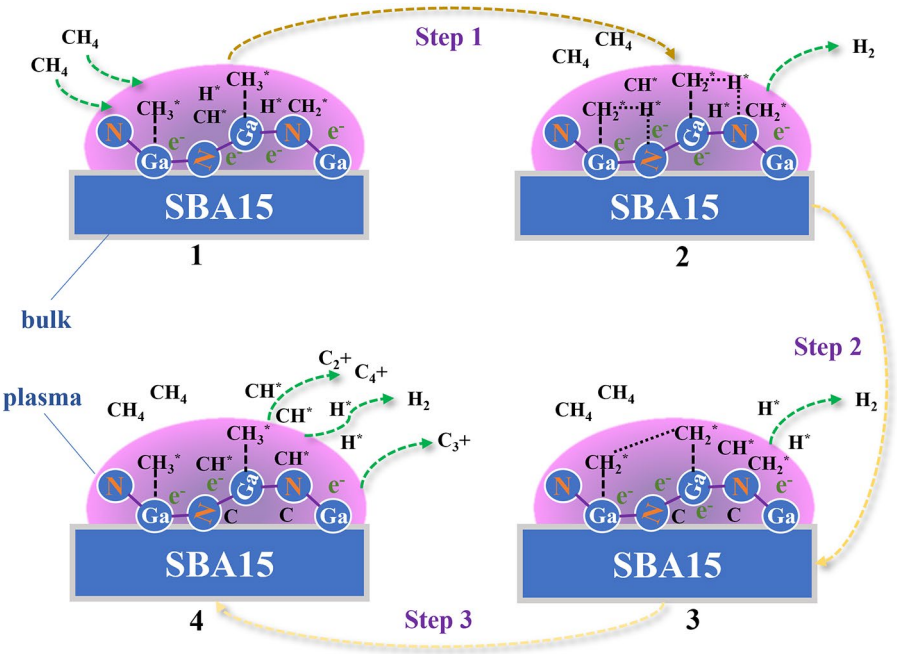

Fig. 10 Reaction pathways for NOCM using plasma catalysis techniques proposed on the GaN/SBA15 surface

neighboring N^{3-}. When hydrogen atoms get adsorbed by nitrogen atoms, they easily dissociate and desorb to generate hydrogen (Step 1). When compared to desorption, the ensuing dehydrogenation of the adsorbed CH_3* on the catalyst surface is far more advantageous. The majority of the adsorbed CH_4 on the Ga-site happened in successive dehydrogenation stages, nitrogen atoms that desorb hydrogen atoms will further adsorb hydrogen atoms from free radicals such as CH_3, which will cause the C-H bonds in the free radicals to stretch and break (Step 2). The cleavage of CH_3* into CH_2* and H* on the Ga-site is the rate-determining step, although the coupling of two CH_2* species to C_2H_4 occurs relatively quickly. Along with less reactive carbon species like CxHy*, the CH_2* intermediate can also generate C_3H_6 and C_3H_8. (Step 3). The latter substance, which has an unknown stoichiometry, may contain polynuclear aromatic compounds. All excess hydrogen atoms are converted to hydrogen in the reactions.

Conclusions

This work produced a dielectric barrier discharge (DBD) plasma paired with a GaN catalyst loaded with SBA15 for the non-oxidative conversion of methane to hydrogen and value-added light hydrocarbons (ethane, ethylene, etc.). Under various discharge powers, methane conversion increases in the plasma only case, while light hydrocarbon products selectivity decreases. In the comparison between plasma + catalysis and plasma-only cases, the findings show that the catalysis greatly accelerates the chemical process. For example, at a discharge

power of 28 W, the methane conversion rises from 27.8 to 39.2%. Moreover, the catalysis performance of different metal loadings was investigated, with 15 wt% catalysis exhibiting the highest methane conversion of 79.4%. However, the selectivity of the C_2+product was only 14.4% and the carbon balance was the lowest among the samples tested, suggesting that the catalyst promoted the production of high chain hydrocarbons such as C_4+.

Further characterization of fresh and spent catalysis allowed for proposing the potential reaction mechanism. Gallium-nitrogen and gallium-oxygen atom pairs acted as Lewis acid-base pairs to promote the decomposition of methane. After the introduction of plasma, the CH_4 molecule produces large amounts of CH_3 and H etc. radicals. The adsorbed C species occurs mainly in successive dehydrogenation steps on the Ga site, where the nitrogen atoms will further adsorb hydrogen atoms from radicals such as CH_3, which results the C-H bonds being stretched and broken. The dehydrogenation produces C_2H_4, etc. as well as less reactive carbon species such as CxHy. For the purpose of converting methane into hydrogen and high-value light hydrocarbons, the activation temperature of CH_4 can be lowered with the help of this catalyst and plasma combination.

Acknowledgements This work was supported by the National Key R&D Program of China (2022YFE0117300), National Natural Science Foundation of China (No. 52276214 and No. 51976191), and the "Pioneer" and "Leading Goose" R&D Program of Zhejiang Province (No. 2023C03129).

Author Contributions Yonggang Gang: Investigation, Formal analysis, Writing - Original Draft. Yanhui Long: Writing - Review & Editing. Kaiyi Wang: Writing - Review & Editing. Yilin Zhang: Validation. Xuping Ren: Validation. Hao Zhang: Conceptualization, Supervision, Formal analysis, Writing - Review & Editing. Xiaodong Li: Supervision, Project administration, Writing - Review & Editing.

Data Availability No datasets were generated or analysed during the current study.

Declarations

Competing Interests The authors declare no competing interests.

References

1. Pakhare D, Spivey J (2014) A review of dry (CO2) reforming of methane over noble metal catalysts[J/OL]. Chem Soc Rev 43(22):7813–7837. https://pubs.rsc.org/en/content/articlelanding/2014/cs/c3cs60395dhttps://doi.org/10.1039/C3CS60395D
2. Performance of 3%Mo/ ZSM-5 catalyst in the presence of water during methane aromatization in supersonic jet expansion - Liu – 2011 - AIChE Journal - Wiley Online Library[EB/OL]. https://aiche.onlinelibrary.wiley.com/doi/https://doi.org/10.1002/aic.12385
3. Global natural gas reserves by country 2020[EB/OL]//Statista. (2023-09-18). https://www.statista.com/statistics/265329/countries-with-the-largest-natural-gas-reserves/
4. Cruchade H, Medeiros-Costa IC, Nesterenko N et al (2022) Catalytic Routes for Direct Methane Conversion to Hydrocarbons and Hydrogen: Current State and Opportunities[J/OL]. ACS Catal 12(23):14533–14558. https://doi.org/10.1021/acscatal.2c03747
5. Al-Fatesh AS, Amin A, Ibrahim AA et al (2016) Effect of Ce and Co Addition to Fe/Al2O3 for Catalytic Methane Decomposition[J/OL]. Catalysts, 6(3): 40(2023-10-08). https://www.mdpi.com/2073-4344/6/3/40. https://doi.org/10.3390/catal6030040
6. Ghoneim SA, El-Salamony RA, El-Temtamy SA (2015) Review on Innovative Catalytic Reforming of Natural Gas to Syngas[J/OL]. World Journal of Engineering and Technology, 4(1): 116–139(2023-09-18). https://www.scirp.org/journal/paperinformation.aspx?paperid=63774. https://doi.org/10.4236/wjet.2016.41011

7. Chawdhury P, Bhargavi KVSS, Subrahmanyam C (2021) A single-stage partial oxidation of methane to methanol: a step forward in the synthesis of oxygenates[J/OL]. Sustainable Energy & Fuels, 5(13): 3351–3362(2023-09-18). https://pubs.rsc.org/en/content/articlelanding/2021/se/d1se00557j. https://doi.org/10.1039/D1SE00557J
8. Xu J, Zhang Y, Xu X et al Constructing La2B2O7 (B=Ti, Zr, Ce) compounds with three typical crystalline phases for the oxidative coupling of methane: the Effect of Phase structures, Superoxide Anions, and alkalinity on the reactivity | ACS Catalysis[EB/OL]. (2023-09-18). https://doi.org/10.1021/acscatal.9b00022
9. Morejudo SH, Zanón R, Escolástico S, Yuste-Tirados I, Malerød-Fjeld H et al Direct conversion of methane to aromatics in a catalytic co-ionic membrane reactor | Science[EB/OL]. (2023-09-18). https://www.science.org/doi/https://doi.org/10.1126/science.aag0274
10. Julian I, Roedern MB, Hueso JL et al (2020) Supercritical solvothermal synthesis under reducing conditions to increase stability and durability of Mo/ZSM-5 catalysts in methane dehydroaromatization[J/OL]. Appl Catal B 263:118360. https://www.sciencedirect.com/science/article/pii/S0926337319311063https://doi.org/10.1016/j.apcatb.2019.118360. (2023-09-18)
11. Dipu AL, Ohbuchi S et al Direct Nonoxidative Conversion of methane to higher hydrocarbons over Silica-Supported Nickel Phosphide Catalyst | ACS Catalysis[EB/OL]. (2023-09-18). https://doi.org/10.1021/acscatal.9b03955
12. Xie P, Pu T, Nie A et al Nanoceria-Supported Single-Atom Platinum Catalysts for Direct Methane Conversion | ACS Catalysis[EB/OL]. (2023-09-18). https://doi.org/10.1021/acscatal.8b00004
13. Guo X, Fang G, Li G, Direct et al Nonoxidative Conversion of Methane to Ethylene, Aromatics, and hydrogen | Science[EB/OL]. (2023-09-18). https://www.science.org/doi/https://doi.org/10.1126/science.1253150
14. Schwach P, Pan X, Bao X (2017) Direct Conversion of Methane to Value-Added Chemicals over heterogeneous catalysts: challenges and Prospects[J/OL]. Chem Rev 117(13):8497–8520. https://doi.org/10.1021/acs.chemrev.6b00715. [2022-09-25]
15. Zhang H, Hensen EJM, Kosinov N 6.14 - Heterogeneous catalysts for the non-oxidative conversion of methane to aromatics and olefins[M/OL]/, /Reedijk J, Poeppelmeier KR, Comprehensive Inorganic Chemistry III (2023) (Third Edition). Oxford: Elsevier, : 311–326(2023-09-18). https://www.sciencedirect.com/science/article/pii/B9780128231449000261. https://doi.org/10.1016/B978-0-12-823144-9.00026-1
16. Li L-Y, Wang Z-Y, Yang S-Y et al Understanding the role of Fe Doping in tuning the size and dispersion of GaN nanocrystallites for CO2-Assisted oxidative dehydrogenation of propane | ACS Catalysis[EB/OL]. (2023-09-18). https://doi.org/10.1021/acscatal.2c01989
17. Dutta K, Shahryari M, Li CJ et al (2023) Elucidation of the CH4 coupling mechanism to C2H4 over GaN catalysts under non-oxidative conditions[J/OL]. Appl Catal A 663:119319. https://www.sciencedirect.com/science/article/pii/S0926860X23002995https://doi.org/10.1016/j.apcata.2023.119319. (2023-09-18)
18. Tang P, Zhu Q, Wu Z et al (2014) Methane activation: the past and future[J/OL]. Energy Environ Sci 7(8):2580–2591. https://doi.org/10.1039/c4ee00604f
19. Erum Mansoor M, Head-Gordon, Alexis T, Bell* Computational modeling of the Nature and Role of Ga species for Light Alkane Dehydrogenation Catalyzed by Ga/H-MFI | ACS Catalysis[EB/OL]. (2023-09-18). https://doi.org/10.1021/acscatal.7b04295
20. Yang Xiao and Arvind Varma Highly Selective Nonoxidative Coupling of Methane over Pt-Bi Bimetallic Catalysts | ACS Catalysis[EB/OL]. (2023-09-18). https://doi.org/10.1021/acscatal.8b00156
21. Bajec D, Kostyniuk A, Pohar A et al (2019) Nonoxidative methane activation, coupling, and conversion to ethane, ethylene, and hydrogen over Fe/HZSM-5, Mo/HZSM-5, and Fe–Mo/HZSM-5 catalysts in packed bed reactor[J/OL]. Int J Energy Res 43(13):6852–6868. https://doi.org/10.1002/er.4697
22. Li L, Mu X, Liu W et al (2014) Thermal non-oxidative aromatization of light alkanes catalyzed by Gallium Nitride[J/OL]. Angew Chem Int Ed 53(51):14106–14109. https://onlinelibrary.wiley.com/doi/abs/10.1002 /anie.201408754. [2023-09-13]
23. Dutta K, Li L, Gupta P et al (2018) Direct non-oxidative methane aromatization over gallium nitride catalyst in a continuous flow reactor[J/OL]. Catal Commun 106:16–19. https://www.sciencedirect.com/science/article/pii/S1566736717304776https://doi.org/10.1016/j.catcom.2017.12.005. (2023-09-18)
24. Dutta K, Shahryari M, Kopyscinski J (2020) Direct nonoxidative methane coupling to Ethylene over Gallium Nitride: a Catalyst Regeneration Study[J/OL]. Ind Eng Chem Res 59(10):4245–4256. https://doi.org/10.1021/acs.iecr.9b05548. [2022-09-27]
25. Khan TS, Balyan S, Mishra S, 等 (2018) Mechanistic insights into the activity of Mo-Carbide clusters for Methane Dehydrogenation and Carbon–Carbon coupling reactions to Form Ethylene in Methane Dehydroaromatization[J/OL]. J Phys Chem C 122(22):11754–11764. https://doi.org/10.1021/acs.jpcc.7b09275. [2022-08-09]

26. Zhang L, Wang ZY, Song J et al (2020) Facile synthesis of SiO2 supported GaN as an active catalyst for CO2 enhanced dehydrogenation of propane[J/OL]. J CO2 Utilization 38:306–313. https://www.sciencedirect.com/science/article/pii/S2212982019313071https://doi.org/10.1016/j.jcou.2020.02.010. [2024-06-15]
27. Paulussen S, Verheyde B, Tu X et al (2010) Conversion of carbon dioxide to value-added chemicals in atmospheric pressure dielectric barrier discharges[J/OL]. Plasma Sources Sci Technol 19(3):034015. https://doi.org/10.1088/0963-0252/19/3/034015. (2023-09-18)
28. Tu X, Whitehead JC (2012) Plasma-catalytic dry reforming of methane in an atmospheric dielectric barrier discharge: understanding the synergistic effect at low temperature[J/OL]. Appl Catal B 125:439–448. https://www.sciencedirect.com/science/article/pii/S0926337312002597https://doi.org/10.1016/j.apcatb.2012.06.006. (2023-09-18)
29. Hsin Liang Chen† HM, Lee‡ S, Chen H, Technology et al [EB/OL]. (2023-09-18). https://doi.org/10.1021/es802679b
30. Chen HL, Lee HM, Chen SH et al (2008) Review of plasma catalysis on hydrocarbon reforming for hydrogen production—Interaction, integration, and prospects[J/OL]. Applied Catalysis B: Environmental, 85(1): 1–9(2023-09-18). https://www.sciencedirect.com/science/article/pii/S0926337308002403. https://doi.org/10.1016/j.apcatb.2008.06.021
31. Neyts EC, Bogaerts A (2014) Understanding plasma catalysis through modelling and simulation—a review[J/OL]. J Phys D 47(22):224010. https://doi.org/10.1088/0022-3727/47/22/224010. (2023-09-18)
32. Tu X, Gallon HJ, Whitehead JC (2013) Plasma-assisted reduction of a NiO/Al2O3 catalyst in atmospheric pressure H2/Ar dielectric barrier discharge[J/OL]. Catal Today 211:120–125. https://www.sciencedirect.com/science/article/pii/S0920586113001259https://doi.org/10.1016/j.cattod.2013.03.024. (2023-09-18)
33. Van Durme J, Dewulf J, Leys C et al (2008) Combining non-thermal plasma with heterogeneous catalysis in waste gas treatment: A review[J/OL]. Applied Catalysis B: Environmental, 78(3): 324–333(2023-09-18). https://www.sciencedirect.com/science/article/pii/S0926337307003037. https://doi.org/10.1016/j.apcatb.2007.09.035
34. Whitehead JC (2010) Plasma catalysis: A solution for environmental problems[J/OL]. Pure and Applied Chemistry, 82(6): 1329–1336(2023-09-18). https://www.degruyter.com/document/doi/10.1351/PAC-CON. DOI:10.1351/PAC-CON-10-02-39
35. Xu C, Tu X (2013) Plasma-assisted methane conversion in an atmospheric pressure dielectric barrier discharge reactor[J/OL]. Journal of Energy Chemistry, 22(3): 420–425(2023-09-18). https://www.sciencedirect.com/science/article/pii/S2095495613600558. https://doi.org/10.1016/S2095-4956(13)60055-8
36. Kim J, Jeoung J, Jeon J, 等 (2019) Effects of dielectric particles on non-oxidative coupling of methane in a dielectric barrier discharge plasma reactor[J/OL]. Chem Eng J 377:119896. https://www.sciencedirect.com/science/article/pii/S1385894718317716https://doi.org/10.1016/j.cej.2018.09.057. (2023-09-18)
37. Sun H, Zhang S, Gao Y et al (2019) Non-oxidative methane conversion in diffuse, filamentary, and spark regimes of nanosecond repetitively pulsed discharge with negative polarity[J/OL]. Plasma Processes and Polymers, 16(8): 1900050(2023-09-18). https://onlinelibrary.wiley.com/doi/abs/10.1002 DOI:10.1002/ppap.201900050
38. Delikonstantis E, Igos E, Augustinus M et al (2020) Sustainable Energy Fuels 4(3):1351–1362. https://pubs.rsc.org/en/content/articlelanding/2020/se/c9se00736ahttps://doi.org/10.1039/C9SE00736A. Life cycle assessment of plasma-assisted ethylene production from rich-in-methane gas streams[J/OL] (2023-09-18)
39. Li XS, Lin CK, Shi C et al (2008) Stable kilohertz spark discharges for high-efficiency conversion of methane to hydrogen and acetylene[J/OL]. Journal of Physics D: Applied Physics, 41(17): 175203(2023-09-18). https://doi.org/10.1088/0022-3727/41/17/175203. DOI:10.1088/0022-3727/41/17/175203
40. Bae J, Lee M, Park S et al (2017) Investigation of intermediates in non-oxidative coupling of methane by non-thermal RF plasma[J/OL]. Catal Today 293–294. https://www.sciencedirect.com/science/article/pii/S0920586117300214https://doi.org/10.1016/j.cattod.2017.01.021. 105–112(2023-09-18)
41. Beloqui Redondo A, Troussard E, van Bokhoven JA (2012) Non-oxidative methane conversion assisted by corona discharge[J/OL]. Fuel Processing Technology, 104: 265–270(2023-09-18). https://www.sciencedirect.com/science/article/pii/S0378382012001932. https://doi.org/10.1016/j.fuproc.2012.05.021
42. Julian I, Ramirez H, Hueso JL, 等 (2019) Non-oxidative methane conversion in microwave-assisted structured reactors[J/OL]. Chem Eng J 377:119764. https://www.sciencedirect.com/science/article/pii/S1385894718316255https://doi.org/10.1016/j.cej.2018.08.150. (2023-09-18)
43. Khoja AH, Tahir M, Amin NAS (2019) Recent developments in non-thermal catalytic DBD plasma reactor for dry reforming of methane[J/OL]. Energy Conv Manag 183:529–560. https://www.sciencedirect.com/science/article/pii/S0196890419300330https://doi.org/10.1016/j.enconman.2018.12.112. (2023-09-18)

44. Chen G, Tu X, Homm G et al (2022) Plasma pyrolysis for a sustainable hydrogen economy[J/OL]. Nat Reviews Mater 7(5):333–334. https://www.nature.com/articles/s41578-022-00439-8https://doi.org/10.1038/s41578-022-00439-8. [2023-10-08]
45. Palraj Kasinathan S, Park WC, Choi et al Plasma-enhanced methane Direct Conversion over particle-size adjusted MOx/Al2O3 (M=Ti and mg) catalysts | SpringerLink[EB/OL]. [2023-10-28]. https://link.springer.com/article/https://doi.org/10.1007/s11090-014-9574-9
46. Lü J, Li Z (2010) Conversion of natural gas to C_2 hydrocarbons via cold plasma technology[J/OL]. J Nat Gas Chem 19(4):375–379. https://www.sciencedirect.com/science/article/pii/S1003995309600827https://doi.org/10.1016/S1003-9953(09)60082-7. [2023-10-28]
47. Li XS, Zhu AM, Wang KJ et al (2004) Methane conversion to C2 hydrocarbons and hydrogen in atmospheric non-thermal plasmas generated by different electric discharge techniques[J/OL]. Catalysis Today, 98(4): 617–624[2022-08-12]. https://www.sciencedirect.com/science/article/pii/S0920586104006145. https://doi.org/10.1016/j.cattod.2004.09.048
48. Scapinello M, Delikonstantis E, Stefanidis GD (2017) The panorama of plasma-assisted non-oxidative methane reforming[J/OL]. Chem Eng Process 117:120–140. https://www.sciencedirect.com/science/article/pii/S0255270116306870https://doi.org/10.1016/j.cep.2017.03.024. [2023-10-28]
49. Mei D, Zhu X, He YL et al (2014) Plasma-assisted conversion of CO_2 in a dielectric barrier discharge reactor: understanding the effect of packing materials[J/OL]. Plasma Sources Sci Technol 24(1):015011. https://iopscience.iop.org/article/https://doi.org/10.1088/0963-0252/24/1/015011. [2023-09-05]
50. Gao M, Zhang Y, Wang H et al (2018) Mode Transition of filaments in packed-Bed Dielectric Barrier Discharges[J/OL]. Catalysts 8(6):248. https://www.mdpi.com/2073-4344/8/6/248https://doi.org/10.3390/catal8060248. [2023-10-08]
51. Tu X, Gallon HJ, Whitehead JC (2011) Transition behavior of packed-Bed Dielectric Barrier discharge in Argon[J/OL]. IEEE Trans Plasma Sci 39(11):2172–2173. https://ieeexplore.ieee.org/document/5975247https://doi.org/10.1109/TPS.2011.2160289. [2023-10-08]
52. Li Wang Y, Yi, Orcid H, Guo, Xin, Tu Atmospheric pressure and Room Temperature Synthesis of Methanol through plasma-catalytic hydrogenation of CO2 | ACS Catalysis[EB/OL]. [2023-09-17]. https://doi.org/10.1021/acscatal.7b02733
53. Jianqi Hao P, Schwach G, Fang et al Enhanced Methane Conversion to Olefins and aromatics by H-Donor molecules under Nonoxidative Condition | ACS Catalysis[EB/OL]. [2023-09-17]. https://doi.org/10.1021/acscatal.9b01771
54. Tu X, Gallon HJ, Twigg MV et al (2011) Dry reforming of methane over a Ni/Al2O3 catalyst in a coaxial dielectric barrier discharge reactor[J/OL]. Journal of Physics D: Applied Physics, 44(27): 274007(2023-09-18). https://doi.org/10.1088/0022-3727/44/27/274007. DOI:10.1088/0022-3727/44/27/274007
55. Chen Y, Mu X, Luo X et al (2020) Catalytic Conversion of Methane at low temperatures: a critical Review[J/OL]. Energy Technol 8(8):1900750. https://onlinelibrary.wiley.com/doi/abs/10.1002 / ente.201900750. [2022-09-20]
56. Trangwachirachai K, Chen CH, Lin YC (2021) Anaerobic conversion of methane to acetonitrile over solid-state-pyrolysis-synthesized GaN catalysts[J/OL]. Mol Catal 516:111961. https://linkinghub.elsevier.com/retrieve/pii/S2468823121005782https://doi.org/10.1016/j.mcat.2021.111961. [2023-09-10]
57. Zong H, Liu X, Meng D et al Effect of Ceria Crystal Plane on the Physicochemical and Catalytic Properties of Pd/Ceria for CO and propane oxidation | ACS Catalysis[EB/OL]. [2023-09-17]. https://doi.org/10.1021/acscatal.5b02617
58. Hu X, Liu Y, Dou L et al (2021) Plasma enhanced anti-coking performance of Pd/CeO2 catalysts for the conversion of methane[J/OL]. Sustainable Energy Fuels 6(1):98–109. https://pubs.rsc.org/en/content/articlelanding/2022/se/d1se01441bhttps://doi.org/10.1039/D1SE01441B. [2023-08-22]
59. Yang G, Han H, Li T et al (2012) Synthesis of nitrogen-doped porous graphitic carbons using nano-CaCO3 as template, graphitization catalyst, and activating agent[J/OL]. Carbon, 50(10): 3753–3765[2023-09-17]. https://www.sciencedirect.com/science/article/pii/S0008622312003120. https://doi.org/10.1016/j.carbon.2012.03.050
60. Zhang L, Wang ZY, Song J et al (2020) Facile synthesis of SiO2 supported GaN as an active catalyst for CO2 enhanced dehydrogenation of propane[J/OL]. J CO2 Utilization 38:306–313. https://www.sciencedirect.com/science/article/pii/S2212982019313071https://doi.org/10.1016/j.jcou.2020.02.010. [2023-09-13]
61. Ravi L, Boopathi K, Panigrahi P et al (2018) Appl Surf Sci 449:213–220. https://www.sciencedirect.com/science/article/pii/S0169433218303313https://doi.org/10.1016/j.apsusc.2018.01.306. Growth of gallium nitride nanowires on sapphire and silicon by chemical vapor deposition for water splitting applications[J/OL][2023-09-17]
62. Xie Z, Yan B, Kattel S et al (2018) Dry reforming of methane over CeO2-supported Pt-Co catalysts with enhanced activity[J/OL]. Appl Catal B 236:280–293. https://www.sciencedirect.com/science/article/pii/S092633731830465Xhttps://doi.org/10.1016/j.apcatb.2018.05.035. [2023-09-17]

63. Wang A, Harrhy JH, Meng S et al (2019) Nonthermal plasma-catalytic conversion of biogas to liquid chemicals with low coke formation[J/OL]. Energy Conv Manag 191:93–101. https://www.sciencedirect.com/science/article/pii/S0196890419304388https://doi.org/10.1016/j.enconman.2019.04.026. [2023-09-17]
64. Chaudhari V, Dutta K, Li CJ et al (2020) Mechanistic insights of methane conversion to ethylene over gallium oxide and gallium nitride using density functional theory[J/OL]. Mol Catal 482:110606. https://www.sciencedirect.com/science/article/pii/S2468823119304559https://doi.org/10.1016/j.mcat.2019.110606. [2023-09-13]